第 36 卷第 5 期
2020 年 5 月

无 机 化 学 学 报
CHINESE JOURNAL OF INORGANIC CHEMISTRY

Vol.36 No.5
949-957

增强多孔纳米红磷的光氧化和光还原性能

马玉花*,# 艾尼娃·木尼热# 朱恩权 粟 智*
(新疆师范大学化学化工学院,乌鲁木齐 830054)

摘要:通过水热法获得了多孔纳米结构的红磷,其中水热处理 24 h 所得的红磷(H-RP24h)具有最高的光催化活性,光氧化罗丹明 B(RhB)和光还原 Cr(Ⅵ)的速率常数分别是 9.2×10^{-2} 和 3.4×10^{-2} min^{-1},是商业红磷的 23 和 26 倍。进一步研究发现水热处理减小了红磷的尺寸、增强了光响应、提高了光生电子和空穴(h^+)的分离,从而提高了它的光催化活性。通过自由基捕获实验发现在光降解反应过程中起主要作用的活性物种是 h^+和超氧自由基。

关键词:红磷;光氧化;光还原;光催化;水热合成
中图分类号:O643.36 **文献标识码**:A **文章编号**:1001-4861(2020)05-0949-09
DOI:10.11862/CJIC.2020.106

Hierarchically Porous Nanosized Red Phosphorus with Enhanced Photo-Oxidation and Photo-Reduction Activities

MA Yu-Hua*,# AINIWA·Munire# ZHU En-Quan SU Zhi*
(*College of Chemistry and Chemical Engineering, Xinjiang Normal University, Urumqi*, 830054, *China*)

Abstract: The as-prepared red phosphorus showed a well-defined complicated porous and nano-sized structure, and the uppermost photocatalytic activity for the hydrothermal treatment 24 h red phosphorus (H-RP24h). The rate constants of the H-RP24h photo-oxidation of rhodamine B (RhB) and photo-reduction of Cr(Ⅵ) were 9.2×10^{-2} and 3.4×10^{-2} min^{-1}, 23 and 26 times superior to those of commercial red phosphorus, respectively. Further studies demonstrated that hydrothermal treatment effectively decreased the size of red phosphorus, enhanced light response, and accelerated the detachment of photogenerated electrons and holes (h^+), thus increased its photocatalytic activity. It was found that the core reactive species in the photodegradation process were h^+ and superoxide ion radicals.

Keywords: red phosphorus; photo-oxidation; photo-reduction; photocatalysis; hydrothermal synthesis

0 Introduction

Semiconductor photocatalysis has been extensively investigated for potential applications in oxidation of organic pollutants[1-7], reduction of heavy metal ions[8-11], and bacterial inactivation[12-14]. During the past few decades, scholars have engaged in the preparation of metal oxide[15-17] and sulfide[18-20] photocatalysts, and various strategies have been taken successively to improve their photocatalytic activity. Nonetheless,

收稿日期:2019-12-02。收修改稿日期:2020-03-10。
新疆维吾尔自治区自然科学基金(No.2019D01B36,2019D01A69)、国家自然科学基金(No.21862022,51968072)、自治区高校科研计划项目(No.XJEDU2018Y030)、自治区“百名青年博士引进计划”天池博士项目(No.BS2017002)、新疆师范大学博士启动项目(No.XJNUB1907)和新疆师范大学“十三五”校级重点学科招标课题(No.17SDK0802)资助。
共同第一作者。
*通信联系人。E-mail:15199141253@163.com,suzhixj@sina.com

above photocatalysts are difficult to apply to practical requests on account of their remarkable cost, complicated preparation process, and easy release of toxic metal ions, et al. Thus, designing efficient, cheap, controllable, and nontoxic photocatalyst has been a hot topic in photocatalysis[21-23]. Recently, nonmetal elemental semiconductors, such as red phosphorus (RP)[24], boron[25], silicon[26], selenium[27], and sulfur[28], have been used to gradually replace conventional photocatalysts because of their special superiority, such as extensive visible-light absorption ability, low price, and common use. RP is a stable semiconductor with a forbidden band width of 1.7 eV and a light absorption range covering almost the entire visible region[29]. It also possesses a suitable conduction band potential (CB) and valence band potential (VB), so it can be used as a potential supreme semiconductor photocatalyst[30-32]. Nevertheless, RP has limited photocatalytic performance due to its low efficiency of photogenerated electrons (e^-) and holes (h^+) separation and transfer, and small specific surface area, et al. Therefore, a feasible method should be developed to spread the e^- and h^+ separation and mobility of RP photocatalysts with nanosized structure.

Several studies have improved the separation and shifted of photogenerated e^- and h^+ by combining RP with other semiconductor photocatalysts. For example, black phosphorus/RP (BP/RP) heterojunction was fabricated through mechanical milling. The conduction band potential of this BP/RP composite photocatalyst is more negative than that of BP, causing photoexcited e^- migrate from CB of RP to CB of BP, so that a large number of photogenerated h^+ remain in the VB position to participate in photodegradation of rhodamine B (RhB) dye[5]. Hereafter, YPO_4, CdS, $Ni(OH)_2$, g-C_3N_4, and graphene were employed to hinder the recombination of photogenerated e^- and h^+ by recombining with RP, thereby improving the photocatalytic efficiency of RP[30,33-36]. However, the limited surface area of RP also negatively affected its application. Rough surface RP was achieved through Co^{2+}-assisted hydrothermal method, and its Brunauer-Emmett-Teller method (BET) surface area is 18 $m^2 \cdot g^{-1}$, which is higher than RP (15 $m^2 \cdot g^{-1}$), but still lower than most nanosized photocatalysts, resulting in fewer reactive sites[37]. Therefore, milling and hydrothermal combined ultrasonic methods have been used to enhance the BET surface area of RP, and top out at 21 $m^2 \cdot g^{-1}$. Thus far, the development of RP-based photocatalysts with large specific surface area and high activity, and exploring their potential applications still remain great challenging.

In this study, the graded porous nanosized RP photocatalyst was obtained from the commercial RP (C-RP) by hydrothermal treatment, then were characterized, and the effect of hydrothermal treatment time on the photocatalytic activity of RP was evaluated by oxidizing RhB and reducing Cr(Ⅵ) under visible-light irradiation. Compared with C-RP, the hydrothermally treated RP (H-RP) exhibited enhanced photocatalytic performance, and the enhanced potential mechanisms were expounded.

1 Experimental

1.1 Preparation of RP photocatalyst

Typically, 0.6 g of C-RP was dispersed in 25 mL deionized water, and then the mixed solution transferred to a 50 mL Teflon-lined stainless autoclave. The autoclave was treated at 200 ℃ for 0 (C-RP), 12 (H-RP12h), 24 (H-RP24h), and 28 h (H-RP28h). The product was separated through centrifugation, washed with deionized water, and dried at 80 ℃ for 4 h.

1.2 Characterization of RP photocatalyst

The phase identification study of the RP was carried out using X-ray diffractometer (XRD, D2, Bruker) in 2θ range of 10°~70°, with Cu $K\alpha$ radiation (λ=0.154 18 nm, tube pressure 50 kV, tube current 200 mA, scanning speed 6° $\cdot$ min^{-1}). The microscopic morphology of the RP was analyzed by scanning electron microscope (SEM, JSM-7610F, Jeol) at an acceleration voltage of 5.0 kV. The diameter of the RP particle was analyzed particle size analyzer (ZS90, Malvern). The morphological and structural of the samples were investigated using transmission electron microscopy (TEM, Tecnai G2 F20 S-TWIN, FEI). The BET surface area was measured from the N_2

adsorption-desorption isotherms using an adsorption apparatus (ASAP 2400, Micromeritics). Light absorption properties of the samples were measured by UV-Vis diffuse reflectance spectroscopy (UV-Vis DRS, Cary 300, Agilent) in the range of 200~800 nm.

1.3 Photocatalytic performance evaluation

The photocatalytic activities of the C-RP, H-RP12h, H-RP16h, H-RP20h, H-RP24h and H-RP28h photocatalysts were estimated by photo-oxidation of RhB and reduction of Cr(Ⅵ) under visible-light irradiation. A 300 W Xe lamp with a cutoff filter (λ>400 nm) was employed as the light source. In a typical experiment, 20 mg of photocatalysts were dispersed in 80 mL RhB (10 mg·L^{-1}) or Cr(Ⅵ) (40 mg·L^{-1}) solutions. Before the irradiation, the adsorption-desorption equilibrium was first achieved by dark adsorption for 30 min under magnetic stirring. Then, the photodegradation experiment was carried out, in which 4 mL of the suspensions was centrifuged at a certain time to remove the photocatalyst. Finally, the remaining concentrations of RhB and Cr(Ⅵ) in the suspension were measured at a wavelength of 554 and 356 nm using a UV-Vis spectrophotometer. The degradation rate was calculated according to formula (**1**):

$$\text{Degradation rate}=C_t/C_0 \quad (1)$$

C_0 is the concentration of the stock solution, and C_t is the concentration of residual pollutants after different times of irradiation.

1.4 Photoelectrochemical measurements

CHI 660E electrochemical workstation was selected to measure the electrochemical performance of the sample in a three-electrode experimental system at ambient temperature. The prepared RP photoelectrodes, Ag/AgCl electrode and Pt electrode appeared as the working electrode, reference electrode and counter electrode, respectively. Working photoelectrodes preparation: 20 mg of prepared photocatalyst added into 1 mL ethanol and was sonicated for 30 min. Then 0.10 mL of sample suspension was dropped onto the conductive side of ITO glass and dried it for 10 h at 40 ℃. Light source: a 300 W Xe lamp with a cutoff filter (λ>400 nm) was employed as the light source. The working electrode and lamp have 30 cm distance. All of the measurements were performed in 0.1 mol·L^{-1} Na_2SO_4 solution. The transient photocurrent measurement was adopted to explore the variations of the photoinduced current density of prepared photocatalyst. Moreover, the EIS test was performed to investigate the charge transfer resistance of photogenerated e^- and h^+ in the dark and light at open circuit potential over the frequency range between 10^5 and 10^3 Hz, with an AC voltage magnitude of 5 mV, using 12 points/decade.

2 Results and discussion

The crystal structures of C-RP and H-RP (H-RP12h, H-RP16h, H-RP20h, H-RP24h and H-RP28h) were examined by XRD (Fig.1a). The XRD patterns of all the RP samples showed peaks at ~15.1° and ~34.2° (2θ), meaning that there was only RP in the sample and no other forms of phosphorus, consistent with the literature[38]. A comprehensive analysis of XRD patterns revealed that the XRD pattern of the H-RP sample was no difference than C-RP, indicating that RP had no impurities and the phase transition did not change significantly in the hydrothermal treatment. Furthermore, the XRD patterns explained that the peak of H-RP was wider than that of C-RP, especially the widest in H-RP24h, suggesting that the hydrothermal treatment RP made the crystal size smaller, and the crystal size of H-RP24h was the smallest. The peak shape of RP gradually sharpened with prolonged holding time, and the sharpest at 24 h. Hence, catalyst crystallization occurred for 24 h.

The size of the RP particle was evaluated using a particle size analyser (Fig.1b). The average particle sizes of C-RP, H-RP20h, H-RP24h, and H-RP28h were 1 987, 283, 92 and 253 nm, respectively. The average particle size of H-RP was more homogeneous and smaller than that of the C-RP particle, and decreased with prolonged hydrothermal treatment holding time. The smallest average particle size was obtained from H-RP24h, which was consistent with the XRD results.

The catalytic performance of a photocatalyst is well known to strongly depend on its morphology. The

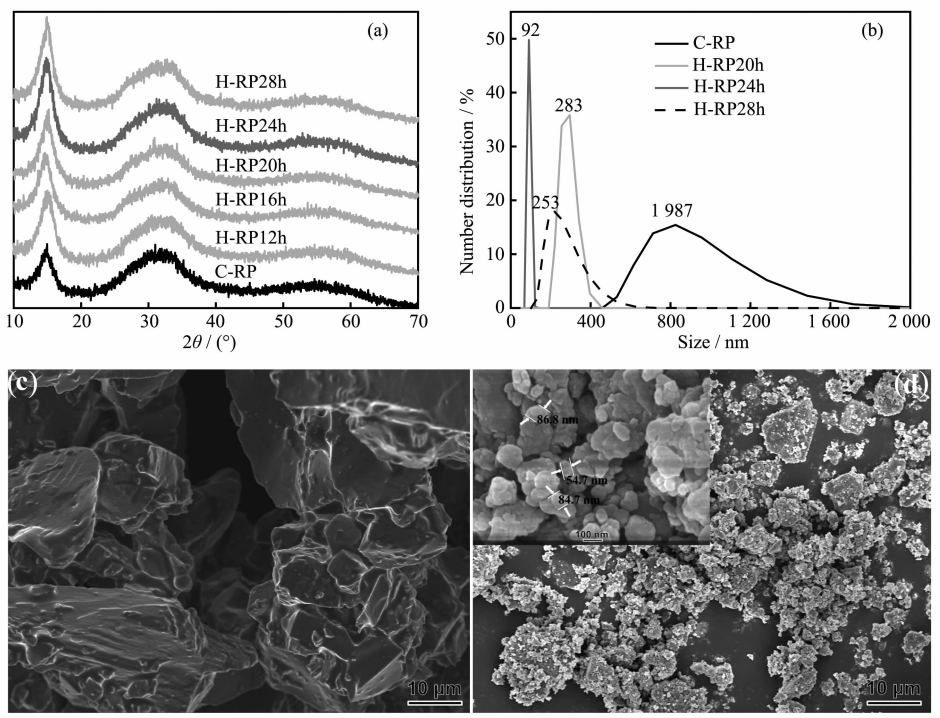

Fig.1 (a) XRD patterns of C-RP, H-RP12h, H-RP16h, H-RP20h, H-RP24h and H-RP28h; (b) Particle size distribution of C-RP, H-RP20h, H-RP24h and H-RP28h; SEM images of (c) C-RP and (d) H-RP24h

representative SEM images of C-RP and H-RP24h were showed in Fig.1(c,d). It was found that the C-RP exhibited a block-like structure, a smooth surface and diameter of about several micrometers (Fig.1c). Comparatively, the surface of RP was rather rough and its particle size was slightly decreased after hydrothermal treated for 24 hours (Fig.1d). The result accorded with the above characterization results. As we known, the small average particle size can induce to the high surface area, more active site and short carrier diffusion distance, which would favourite to enhance the photocatalytic activity of a photocatalyst.

Fig.2 showed the TEM images. From Fig.2a and 2b, the C-RP particles exhibited smooth surface and micron diameter. While, the surface of the H-RP24h was rough, and many pores of several to tens of nanometers were found to be randomly distributed, which can provide a quantity of active sites, also improve the effective separation and transmission of photogenerated e^- and h^+. By enlarging the TEM image, the size of the H-RP24h was reduced to the nanometer range, indicating an increase in surface area. These results clearly showed that the hydrothermal treatment of RP increased the crystallinity and reduced the size, which is very favourable for photocatalytic reaction.

The particle size analyzed result showed that the H-RP24h photocatalyst possessed smallest average size, leading to high surface area. The specific surface area of C-RP and H-RP24h were further tested through N_2 adsorption-desorption measurements (Fig. 3a). The result displayed that the N_2 adsorption-desorption isotherms of C-RP and H-RP24h were type IV with hysteresis loops of type H3 classification. The surface area of H-RP24h was 28 $m^2 \cdot g^{-1}$, 4 times higher than that of C-RP (7 $m^2 \cdot g^{-1}$). The surface of photocatalyst as bridge connected between photocatalyst and dye. Therefore, the larger it is, and the more adsorption and active sites. Pore size distribution curve (Fig.3b) exhibited that pore size of the H-RP24h were richer than that of C-RP. Above results explained clearly that the H-RP24h photocatalyst had huge surface area and abundant pore size, which could result in more active sites and easier reactant transport, thus improving the photocatalytic activity of RP.

The RhB and Cr(Ⅵ) were selected as two typical

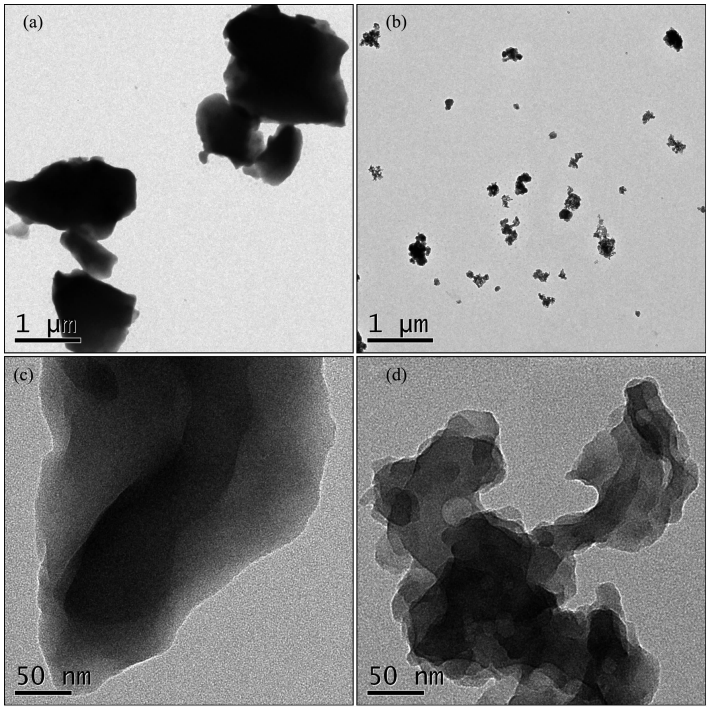

Fig.2　TEM images of (a, c) C-RP and (b, d) H-RP24h

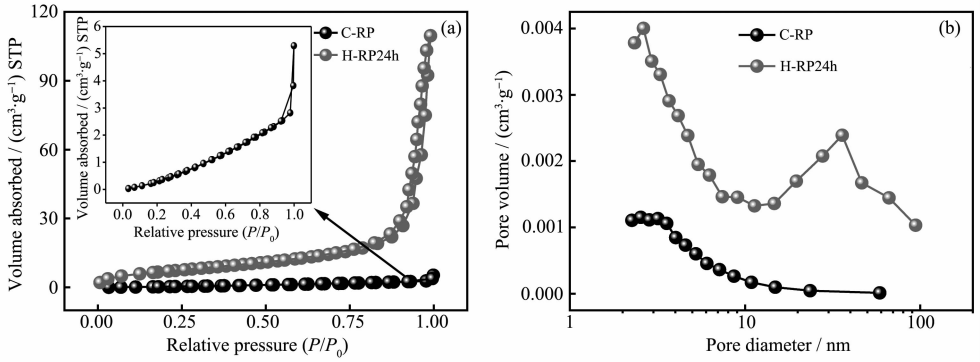

Fig.3　(a) N_2 adsorption-desorption isotherms and (b) corresponding pore size distribution curves of C-RP and H-RP24h

recalcitrant model pollutants to monitor the photo-oxidation and photo-reduction of the C-RP and H-RP with/without visible-light irradiation. The results of pollutant stability experiments showed that neither RhB nor Cr(Ⅵ) degraded under visible-light without photocatalyst, indicating that the two selected model pollutants have high stability. In darkness, it was estimated the adsorption abilities of C-RP, H-RP12h, H-RP12h, H-RP16h, H-RP20h, H-RP24h and H-RP28h photocatalyst to RhB and Cr(Ⅵ) (Fig.4a and b), and found that the adsorption ability of photocatalyst increased with the extension of hydrothermal time and decreased after reaching the highest value. The highest adsorption activity was obtained from the H-RP24h photocatalyst. The adsorption rates of Cr(Ⅵ) and RhB by H-RP24h photocatalyst were 55% and 33% respectively. After the photocatalyst was added to the photodegradation system, the photo-oxidation rates increased with prolonged visible-light irradiation time, reaching 14%, 79%, 87%, 93%, 98% and 93% in 40 min with C-RP, H-RP12h, H-RP16h, H-RP20h, H-RP24h, and H-RP28h to RhB, respectively (Fig.4a). Similar trends had also been obtained for the photo-reduction of Cr(Ⅵ), and photo-reduction rates were 9%, 26%, 64%, 75%, 92% and 72% in 70 min with C-RP, H-RP12h, H-RP16h, H-RP20h, H-RP24h, H-RP28h, respectively (Fig.4b). The results clearly showed that the highest photo-oxidation and photo-

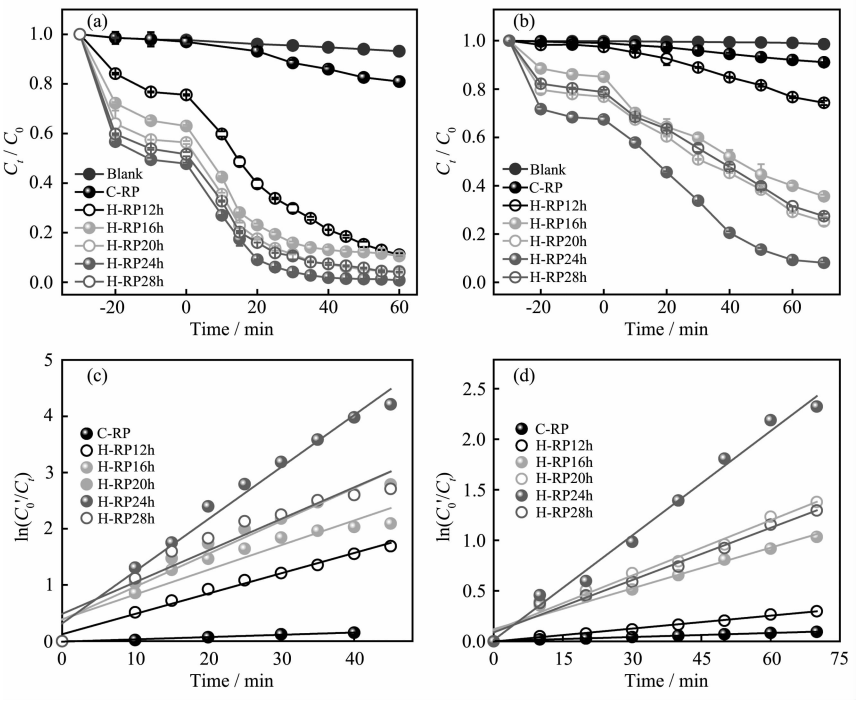

Fig.4 Degradation of (a) RhB and (b) Cr(Ⅵ) by C-RP, H-RP12h, H-RP16h, H-RP20h, H-RP24h and H-RP28h; Reaction kinetics for (c) RhB and (d) Cr(Ⅵ) degradation

reduction activities were obtained from H-RP24h for RhB and Cr(Ⅵ).

Reaction kinetic implied that the photodegradation of the two pollutants well fitted with the pseudo-first-order model:

$$\ln(C_0'/C_t)=kt$$

Where k is the apparent rate constant (min^{-1}), C_0' is the concentration of pollutant after adsorption-desorption equilibrium, C_t is the residual concentration of the pollutant at certain time intervals under visible-light irradiation.

Fig.4(c,d) present the k of C-RP and the hydrothermally treated RP for the photo-oxidation RhB and photo-reduction Cr(Ⅵ). Indicating that the k values increased with prolonged hydrothermal treatment time and then decreased, H-RP24h exhibited considerably higher degradation rates. The k values were 9.2×10^{-2} and 3.4×10^{-2} min^{-1} for RhB and Cr(Ⅵ), which were approximately 23 and 26 times higher than those of C-RP, respectively. This finding indicated that hydrothermal treatment could improve the photo-oxidation and photo-reduction activities of C-RP. The control of the hydrothermal treatment time is crucial for obtaining the best photocatalytic activity. It was found that the H-RP24h possessed excellent photocatalytic performance than other reported RP-based photocatalysts either for the photo-oxidation of RhB or photo-reduction of Cr(Ⅵ)[4-5,21,39].

After the reaction, the H-RP24h photocatalysts were recovered by centrifuging, washing, drying and then was cycled for degradation of the RhB under the same reaction conditions. The photocatalytic photo-oxidation efficiency was 97% for the first degradation, then after five consecutive photocatalytic oxidation cycles, the photocatalytic efficiency mildly reduced from 97 to 94%. The result can be blamed to the adsorption of RhB by the catalyst, resulting in a decrease in adsorption and active sites on its surface. Above results suggested that the prepared H-RP24h photocatalyst exhibited high cycle photocatalytic performance and could be used as an efficient and stable visible-light photocatalyst.

The characteristic and experimental results exhibited that the hydrothermal treatment could meaningfully enhance the photocatalytic activity of RP. So it was meaningful to investigate the light

absorption, charge transfer properties of C-RP and H-RP24h and the principal active specie to explain the potential mechanism.

The light absorption properties of C-RP and H-RP24h were analysed (Fig.5a), and the result showed the light response range contained almost the ultraviolet and the entire visible region (200~750 nm), highlighting the potential applications for the visible-light-driven photocatalytic reactions. Compared with C-RP, the light absorption peak of H-RP24h was blue-shifted due to the decrease of particle size, but the light absorption intensity was enhanced. The characterization results showed that the hydrothermal treatment can enhance the optical properties of RP. The result can be interpreted that with the extension of the time of hydrothermal treatment, diameter of RP decreased into nanoscale, which made the electrons were confined, resulting in that the band gap energy (E_g) between CB and VB was increased ($E_{g,\ H\text{-}RP24h}$=1.77 eV, $E_{g,\ C\text{-}RP}$=1.61 eV). Therefore, the absorption spectrum shifted toward the blue region. Similar phenomenon had been found in previous studies[24].

The photoresponse ability and photogenerated e^- and h^+ recombination are essential for the enhancement of the photocatalytic effect of photocatalyst. So in this experiment, transient photocurrent measurement was used to investigate above performance of the C-RP and H-RP24h photocatalysts, the results were shown in Fig.5b. Both of the samples produced photoelectron under visible light irradiation and clearly presented stable, rapid and reversible photocurrent response. Furthermore, the photocurrent value for H-RP24h was 1.5 $\mu A \cdot cm^{-2}$, six times higher than that of C-RP electrode (0.25 $\mu A \cdot cm^{-2}$). The higher photocurrent density indicated stronger photo to electronic conversion capacity and higher efficient separation of photogenerated e^- and h^+ of H-RP24h than that of C-RP.

The separation ability and the charge transfer resistance of photogenerated e^- and h^+ of the photocatalyst were further verified by electrochemical impedance. As shown in Fig.5c, the arc radius of H-RP24h photocatalyst was smaller than that of C-RP whether visible-light irradiation or dark, indicating that the conveying of photogenerated e^- and h^+ was less obstructed. For the photocatalytic oxidation and reduction over a photocatalyst, photogenerated e^- and

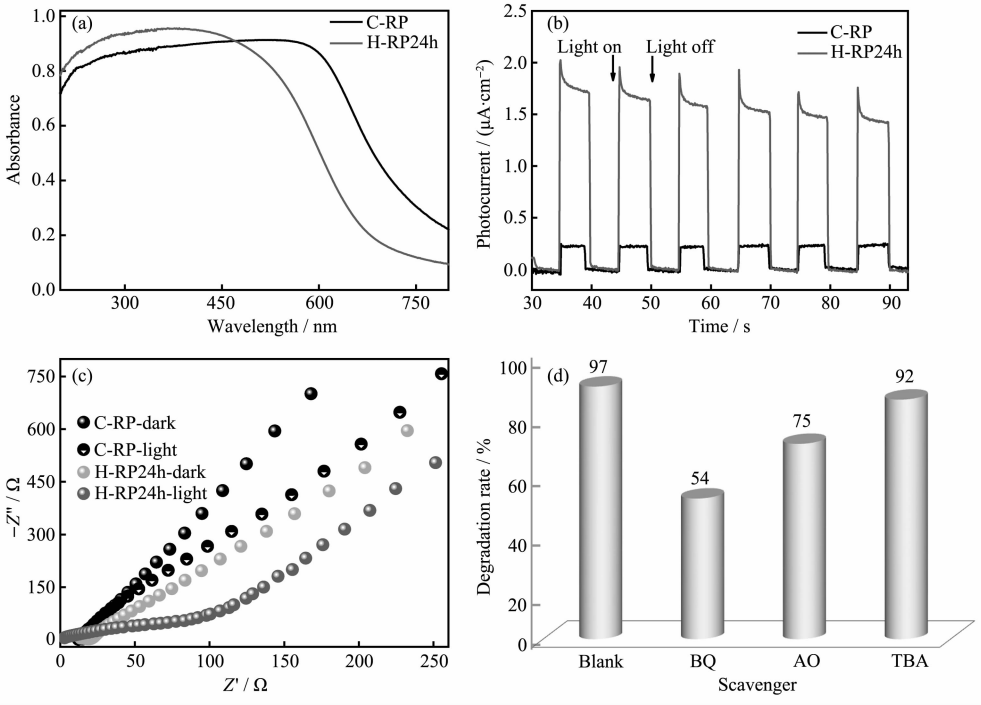

Fig.5 (a) UV-Vis DRS spectra of C-RP and H-RP24h, (b) photocurrent response of C-RP and H-RP24h, (c) electrochemical impedance spectra of C-RP and H-RP24h and (d) effect of different radical scavengers on the degradation efficiency of RhB for H-RP24h

h^+ pairs can detach and separately transfer to the surface to take part in photocatalytic reduction/oxidation reaction.

A series of free radical trapping experiments were organized to investigate the mechanism of H-RP24h degradation for RhB. The quencher of h^+, hydroxyl radical (·OH), and superoxide radical ($\cdot O_2^-$) were 20 mmol·L^{-1} ammonium oxalate (AO), tert-butyl alcohol (TBA), and benzoquinone (BQ), respectively. As shown in Fig.5d, with the addition of BQ and AO, the photodegradation rates were decreased quickly from 97% to 54% and 75% for the H-RP24h photodegration of RhB, respectively. While, the degradation efficiency was little change (97% to 92%) in the presence of TBA, implying the $\cdot O_2^-$ and h^+ were the main reactive species in the H-RP24h photocatalyst reaction system.

On the basis of the Mott-Schottky equation, the flat-band positions of the H-RP24h was −0.66 V, the E_{CB} of a semiconductor can be approximately underestimated to be equal to its flat band potential[40], so the E_{CB} of H-RP24h was estimated to be −0.66 V. Hence, the E_{VB} was calculated to be 1.11 V ($E_{VB}=E_{CB}+E_g$)[41]. Combined with experimental results and discussion, the potential mechanism for the photo-oxidation and photo-reduction of pollutants with H-RP24h photocatalyst was put forward. Firstly, the Cr(Ⅵ) and RhB pollutants were adsorbed by the photocatalyst. Secondly, the reaction system absorbed photons and then generated countless e^- and h^+ by the excited RP. The photogenerated e^- transferred from VB to CB and to photo-reduction of Cr(Ⅵ), partials were captured by O_2 to yield $\cdot O_2^-$, because the E_{CB} of H-RP24h was negative than the $\cdot O_2^-/O_2$ potential (−0.33 V)[21]. Simultaneously, the abundant h^+ was left in VB, while the E_{VB} is inadequate for oxidizing H_2O to ·OH (2.38 V)[21]. Finally, the $\cdot O_2^-$ and the left h^+ were combined to photo-oxidation of RhB into H_2O, CO_2 and other inorganic salts.

3 Conclusions

Hierarchically porous nanosized RP was prepared via a low-cost hydrothermal method with an earth-abundant C-RP. The hydrothermally treated RP exhibited a remarkably high photocatalytic activity, especially the H-RP24h photocatalyst displayed the highest photo-oxidation and photo-reduction performance. The k values were 9.2×10^{-2} and 3.4×10^{-2} min^{-1} for RhB and Cr(Ⅵ), which were approximately 23 and 26 times higher than that of C-RP, respectively. Given its hierarchically porous structure, nano particle size and high specific surface area, H-RP24h exhibited stronger photo to electronic conversion capacity and more efficient separation of photogenerated e^- and h^+. Additionally, The H-RP24h photocatalyst also showed high stability and reusability (96% of its initial photoactivity after five runs). Therefore, this hierarchically porous nanosized RP photocatalyst demonstrated immense potential application for the treatment of environmental pollutants.

References:

[1] Li H L, Chen Y J, Zhou W, et al. *Appl. Surf. Sci.*, **2019**,**470**:631-638

[2] Yuan X J, Floresyona D, Aubert P H, et al. *Appl. Catal. B*, **2019**,**242**:284-292

[3] Ma J F, Liu Q, Zhu L F, et al. *Appl. Catal. B*, **2016**,**182**:26-32

[4] Chan D K L, Yu J C, Li Y C, et al. *J. Environ. Sci.*, **2017**, **60**:91-97

[5] Shen Z R, Sun S T, Wang W J, et al. *J. Mater. Chem. A*, **2015**,**3**:3285-3288

[6] Lin T, Jia W J, Ming Z G, et al. *J. Hazard. Mater.*, **2016**, **306**:295-304

[7] Deng Y C, Tang L, Zeng G M, et al. *Appl. Surf. Sci.*, **2016**, **387**:882-893

[8] Pu S Y, Hou Y Q, Chen H Y, et al. *Catalysts*, **2018**,**8**:251-268

[9] Chen F, Yang Q, Wang Y L, et al. *Chem. Eng. J.*, **2018**,**348**:157-170

[10]Qiu J H, Zhang X F, Zhang X G, et al. *J. Hazard. Mater.*, **2018**,**349**:234-241

[11]Zhang G Q, Chen D Y, Li N, et al. *Appl. Catal. B*, **2018**, **232**:164-174

[12]Wang T Q, Jiang Z F, An T C, et al. *Environ. Sci. Technol.*, **2018**,**52**:4774-4784

[13]Xia D H, He H J W, Liu H D, et al. *Appl. Catal. B*, **2018**,

238:70-81

[14]Wang W J, Li G Y, An T C, et al. *Appl. Catal. B*, **2018**,**238**:126-135

[15]Yu Z B, Chen X Q, Kang X D, et al. *Adv. Mater.*, **2018**,**30**:1706259-1706266

[16]Karthik K, Dhanuskodi S, Gobinath C, et al. *J. Mater. Sci.: Mater. Electron.*, **2018**,**29**:5459-5471

[17]Leow W R, Yu J C, Li Y B, et al. *Angew. Chem. Int. Ed.*, **2018**,**57**:9780-9784

[18]Jin J, Yu J G, Guo D P, et al. *Small*, **2015**,**11**:5262-5271

[19]Strataki N, Antoniadou M, Dracopoulos V, et al. *Catal. Today*, **2010**,**151**:53-57

[20]Xu J, Cao X J. *Chem. Eng. J.*, **2015**,**260**:642-648

[21]Bai X, Wan J, Jia J, et al. *Mater. Lett.*, **2018**,**222**:187-191

[22]Hu S Z, Ma L, You J G, et al. *RSC Adv.*, **2014**,**4**:21657-21663

[23]Pirhashemi M, HabibiYangjeh A, Rahim Pouran S. *J. Ind. Eng. Chem.*, **2018**,**62**:1-25

[24]Ren Z P, Li D H, Xue Q, et al. *Catal. Today*, **2020**,**340**:115-120

[25]Liu G, Yin L C, Niu P, et al. *Angew. Chem. Int. Ed.*, **2013**, **52**:6242-6245

[26]Kang Z H, Tsang C H A, Wong N B, et al. *J. Am. Chem. Soc.*, **2007**,**129**:12090-12091

[27]Chiou Y D, Hsu Y J. *Appl. Catal. B*, **2011**,**105**:211-219

[28]Peng W C, Li X Y. *Nano Res.*, **2013**,**6**:286-292

[29]Wang F, Ng W K H, Yu J C, et al. *Appl. Catal. B*, **2012**, **111-112**:409-414

[30]Jing L, Zhu R X, Phillips D L, et al. *Adv. Funct. Mater.*, **2017**,**27**:1703484-1703492

[31]Pfitzner A. *Angew. Chem. Int. Ed.*, **2006**,**45**:699-700

[32]Ansari S A, Cho M H. *Sci. Rep.*, **2016**,**6**:25405-25415

[33]Wang F, Li C H, Li Y C, et al. *Appl. Catal. B*, **2012**,**119-120**:267-272

[34]Shi Z S, Dong X F, Dang H F. *Int. J. Hydrogen Energy*, **2016**,**41**:5908-5915

[35]Dang H F, Dong X F, Dong Y C, et al. *RSC Adv.*, **2014**,**4**:44823-44826

[36]Li W B, Zhang Y P, Tian G D, et al. *J. Mol. Catal. A: Chem.*, **2016**,**423**:356-364

[37]Li W B, Yue J G, Hua F X, et al. *Mater. Res. Bull.*, **2015**, **70**:13-19

[38]Ma Y H, Tuniyazi D L X, Ainiwa M N R, et al. *Mater. Lett.*, **2020**,**262**:127023-127026

[39]Wang J, Zhang D K, Deng J K, et al. *J. Colloid Interface Sci.*, **2018**,**516**:215-223

[40]Xu D F, Cheng B, Cao S W, et al. *Appl. Catal. B*, **2015**, **164**:380-388

[41]Yang S B, Xu D B, Chen B Y, et al. *Appl. Surf. Sci.*, **2016**, **383**:214-221